Wetting of a spherical particle by a nematic liquid crystal

Jun-ichi Fukuda*
Yokoyama Nano-structured Liquid Crystal Project, ERATO, Japan Science and Technology Agency, 5-9-9 Tokodai, Tsukuba 300-2635, Japan

Holger Stark
Fachbereich Physik, Universität Konstanz, D-78457 Konstanz, Germany

Hiroshi Yokoyama
Yokoyama Nano-structured Liquid Crystal Project, ERATO, Japan Science and Technology Agency, 5-9-9 Tokodai, Tsukuba 300-2635, Japan
and Nanotechnology Research Institute, AIST, 1-1-1 Umezono, Tsukuba 305-8568, Japan
(Received 10 July 2003; published 27 February 2004)

We discuss how the curvature of a substrate influences wetting by a nematic liquid crystal concentrating on the surface of a spherical particle. Our investigation is based on Landau–de Gennes free energy formulated in terms of second-rank nematic order parameter Q_{ij}. We review the method to treat wetting transitions in curved geometries and calculate the wetting phase diagram in terms of the temperature and a surface coupling parameter. We find that the length of the prewetting line which corresponds to the boundary-layer transitions introduced by Sheng [Phys. Rev. A **26**, 1610 (1982)] gradually decreases with a decrease in particle radius until it vanishes completely below a critical radius of about 100 nm. The prewetting line ends at a critical point which we study in detail. By interpreting the effect of curvature as an effective shift in temperature in Landau–de Gennes theory, we are able to formulate a good estimate for the critical temperature as a function of the inverse particle radius. It demonstrates that splay deformations around the particle significantly influence nematic wetting of curved surfaces.

DOI: 10.1103/PhysRevE.69.021714 PACS number(s): 61.30.Hn, 64.70.Md, 61.30.Cz, 82.70.Dd

I. INTRODUCTION

The wetting of surfaces by a fluid has tremendous industrial applications as exemplified by the famous Lotus effect [1]. For three decades, wetting has been intensively studied [2,3] and, in connection with nanostructuring of surfaces and microfluidic, it gains further importance. In his seminal paper [4], Cahn argued on the basis of mean-field theory that a two-phase system moving along the coexistence line towards its critical point exhibits complete wetting beyond the wetting temperature T_w. Furthermore, a prewetting line exists which starts on the coexistence curve at T_w and ends at a critical point located in the region of either phase 1 or 2. Cahn's work was extended [5] and then wetting of curved surfaces of cylinders and spheres was studied [6–9], also within density-functional theory [10]. The main features are that complete wetting cannot occur on curved surfaces and that the prewetting line vanishes with increasing curvature. Experimental observations of wetting phenomena on spheres and cylinders are reported in Refs. [11] and [12].

Surface phenomena in liquid crystals are widely studied [13,14] partly due to their importance in liquid crystal displays. Sheng was the first to investigate the so-called boundary-layer transition in nematic liquid crystals close to a planar substrate and above the isotropic–nematic phase transition [15]. It corresponds to the prewetting transition mentioned above. Detailed investigations were then performed by Poniewierski and Sluckin [16,17] who also elaborated upon the connection to wetting. Experiments confirm the surface induced nematic order [18,19] and recently the boundary-layer transition was observed [20]. Numerical studies and density functional theory established complete orientational wetting [21].

In this article we report on the effect of curvature on nematic wetting layers. Our work is stimulated by recent investigations of surface-induced nematic order around colloidal particles and their effect on the stability of colloidal dispersions [22–24]. So far theoretical studies have been based on the harmonic approximation of the Landau–de Gennes free energy functional. Here, we will employ complete Landau–de Gennes theory to study orientational wetting around a spherical particle. Since the conventional method to treat wetting transitions in planar geometries [4,15] is no longer applicable for systems with curved boundaries, we will apply a method outlined in Refs. [6,8], and [9].

The results of our investigation are summarized in Fig. 1, where we plot the prewetting line for different reduced particle radii as a function of the temperature and surface-coupling parameter w, also called the surface-ordering field. Let us first review the planar geometry [15] (that corresponds to an infinite particle radius) and place it within the context of wetting. At temperatures well above the reduced bulk-transition temperature $\tau_{\mathrm{IN}}=0.125$, the nematic scalar order parameter $\bar{Q}_0$ at the surface assumes its small ''thin-layer'' value. When traversing τ_{IN} for $w<0.037$, it jumps to a value closer to that of nematic bulk parameter $\bar{Q}_b$. In the treatment by Cahn [4], this corresponds to a situation where the nem-

*Electronic address: fukuda@nanolc.jst.go.jp

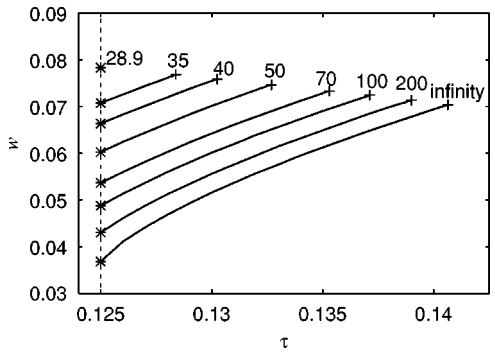

FIG. 1. Prewetting lines for different reduced particle radii $\bar{R}_0$ (see numbers close to the plus signs) as a function of temperature τ and surface-coupling parameter w. The lines start at the bulk phase transition temperature $\tau_{\mathrm{IN}}=1/8$ and end at critical points (τ^*,w^*) indicated by the plus sign. Surface-layer transitions do not occur below $\bar{R}_0=28.9$.

atic phase only partially wets the surface. When $w>0.037$, the surface order parameter exhibits a boundary-layer transition at the prewetting line where it jumps from its thin-layer to the larger ''thick-layer'' value. The prewetting line ends at a critical point (τ^*,w^*) indicated by a plus sign. For $w>w^*$, the surface order parameter behaves smoothly with a decrease in temperature. Following the analysis of Cahn [4], the nematic phase completely wets the bounding surface at τ_{IN} if w is chosen larger than the so-called wetting surface-coupling parameter $w_m=0.037$ [25] introduced in full analogy to the wetting temperature. To see this we note that at τ_{IN} the thick-layer value of the surface order parameter is always larger than the bulk value $\bar{Q}_b$. So between the substrate and isotropic phase, we can fill in a macroscopically thick layer of nematic phase, i.e., complete wetting. Now, Fig. 1 clearly indicates the effect of curvature on the boundary-layer transition. The length of the prewetting line gradually decreases with a decrease in particle radius and the line completely vanishes below a reduced critical radius of $\bar{R}_0^*=28.9$, corresponding to 100 nm for a typical nematic mesogen. As a further effect of curvature, we observe that complete wetting at τ_{IN} is suppressed since the surface tension at the interface between the nematic and isotropic phases grows according to the square of the distance from the center of the sphere. We will demonstrate in this article that, compared to wetting with, e.g., binary fluids, elastic distortion of the director field close to the particle surface has a pronounced effect on the wetting properties of nematic liquid crystals.

In the following, we review theory needed to calculate the phase diagram of Fig. 1 (Sec. II) and then discuss details of our results (Sec. III). We finish with a conclusion (Sec. IV) where we suggest extensions of the present work and comment on experimental verification.

II. DESCRIPTION OF THE MODEL

A. Free energy

We begin with a description of our model by writing the free energy of the system in terms of the local orientational order parameter of a nematic liquid crystal for which we adopt the second-rank symmetric and traceless tensor $Q_{\alpha\beta}(\boldsymbol{r})$ [26], also called the alignment tensor [27]. The free energy density f_{bulk} of a nematic liquid crystal in the bulk is given by the sum of the local and elastic energy. We write the former in terms of Landau–de Gennes expansion [26] as $f_{\mathrm{local}}=(1/2)AQ_{\alpha\beta}^2-(1/3)BQ_{\alpha\beta}Q_{\beta\gamma}Q_{\gamma\alpha}+(1/4)C(Q_{\alpha\beta}^2)^2$, with A,B and C phenomenological coefficients. Greek indices denote Cartesian coordinates and summation over repeated indices is implied. For simplicity, we adopt the one-constant form of the elastic energy as $f_{\mathrm{el}}=(1/2)L_1(\partial_\gamma Q_{\alpha\beta})^2$, where L_1 is the elastic constant.

The phenomenological surface free energy density f_s describes the capability of the bounding surfaces to induce orientational order right at the surface. In this article, following the work of Sheng [15], we employ the simple form $f_s=-WQ_{\alpha\beta}\nu_\alpha\nu_\beta$, where the phenomenological surface-coupling parameter W, also called the surface-ordering field, characterizes the strength of anchoring and ν_α is the unit vector normal to the surface. This surface energy is a straightforward generalization of that used by Sheng [15], who discussed the boundary-layer transition of a nematic on a flat substrate. The minus sign in front of $W>0$ implies that at the surface homeotropic ordering is preferred. We adopt this simple surface energy because one of the aims of this article is a concise presentation of the method needed to treat the effect of curvature on the boundary-layer transition. Based on the present investigation, more general types of surface free energy that contain, e.g., quadratic terms in $Q_{\alpha\beta}$, can be studied.

The total free energy of the system is now written as $F=\int_V d^3\boldsymbol{r}f_{\mathrm{bulk}}+\int_S d^2\boldsymbol{r}f_s$, where V is the volume occupied by the liquid crystal and S denotes the bounding surfaces. To simplify the discussion below, we use reduced quantities. We rescale the orientational order parameter to $Q_{\alpha\beta}=s\bar{Q}_{\alpha\beta}$ with $s=2\sqrt{6}B/9C$ and write all lengths in units of $\xi_n\equiv\sqrt{L_1/Cs^2}=\sqrt{27L_1C/8B^2}$, where $2\sqrt{2}\xi_n$ denotes the nematic coherence length at the isotropic–nematic phase transition. The rescaled free energy of the system then reads

$$\frac{F}{{\xi_n}^3\Delta f}=\int d^3\bar{\boldsymbol{r}}\left\{\frac{1}{2}\tau\bar{Q}_{\alpha\beta}^2-\frac{\sqrt{6}}{4}\bar{Q}_{\alpha\beta}\bar{Q}_{\beta\gamma}\bar{Q}_{\gamma\alpha}+\frac{1}{4}(\bar{Q}_{\alpha\beta}^2)^2+\frac{1}{2}(\bar{\partial}_\gamma\bar{Q}_{\alpha\beta})^2\right\}-\int d^2\bar{\boldsymbol{r}}\bar{w}\bar{Q}_{\alpha\beta}\nu_\alpha\nu_\beta, \tag{1}$$

where $\bar{\boldsymbol{r}}=\boldsymbol{r}/\xi_n$, $\bar{\partial}_\gamma=\xi_n\partial_\gamma$ and $\tau\equiv A/Cs^2=27AC/8B^2$ gives the reduced temperature. The unit of the free energy $\Delta f\equiv Cs^4=64B^4/729C^3$ is proportional to the latent heat and the reduced anchoring strength is defined as $w\equiv W\xi_n/L_1s$.

In this article we consider the effect of one spherical particle on the phase transition behavior of a nematic liquid crystal close to the particle's surface. We place the center of the sphere at the origin and denote the radius by $R_0=\bar{R}_0\xi_n$. According to the symmetry of the system, we choose the uniaxial order-parameter profile $\bar{Q}_{\alpha\beta}(\bar{\boldsymbol{r}})=\bar{Q}(\bar{r})\times(\hat{e}_\alpha^r\hat{e}_\beta^r-\frac{1}{3}\delta_{\alpha\beta})$, where $\hat{\boldsymbol{e}}^r$ is the unit vector along the radial

direction (that represents the nematic director) and the scalar order parameter $\bar{Q}(\bar{r})$ only depends on $\bar{r}$, the (reduced) distance from the center of the particle. With this choice, the free energy of Eq. (1) is then written in terms of $\bar{Q}(\bar{r})$ as

$$\bar{F} \equiv \frac{3F}{8\pi\xi_n R_0^2 \Delta f} = \frac{1}{\bar{R}_0^2}\int_{\bar{R}_0}^{\infty} d\bar{r}\,\bar{r}^2 \left\{ \bar{f}(\bar{Q}) + 3\left(\frac{\bar{Q}}{\bar{r}^2}\right) + \frac{1}{2}\left(\frac{d\bar{Q}}{d\bar{r}}\right)^2 \right\} - w\bar{Q}|_{\bar{r}=\bar{R}_0}, \tag{2}$$

with the bulk local energy $\bar{f}$ in terms of $\bar{Q}$ being

$$\bar{f}(\bar{Q}) = \frac{1}{2}\tau\bar{Q}^2 - \frac{\sqrt{6}}{12}\bar{Q}^3 + \frac{1}{6}\bar{Q}^4. \tag{3}$$

Note that the second term of the integrand in Eq. (2) is associated with splay deformation of the orientational order around the spherical particle. It is specific to a nematic liquid crystal and therefore absent in similar investigations of wetting in a binary fluid whose composition is specified by a scalar order parameter [9]. In addition, this second term can be viewed as an effective shift in temperature, depending on radial coordinate $\bar{r}$.

For later use, we summarize the properties of the bulk isotropic–nematic transition deduced from the local free energy (3). The bulk isotropic–nematic phase transition occurs at reduced temperature, $\tau_{\mathrm{IN}} = 1/8$, and the nematic order parameter at the point of transition is $\bar{Q}_{\mathrm{IN}} = \sqrt{6}/4 \simeq 0.612$. The metastable nematic phase exists in the temperature range of $\tau_{\mathrm{IN}} < \tau < 9/64$ with a limiting order parameter of $\bar{Q}_* = 3\sqrt{6}/16 \simeq 0.459$ at the superheating temperature, $\tau = 9/64$. Finally, the isotropic phase becomes unstable at the supercooling temperature, $\tau = 0$.

B. Determination of the order-parameter profile and phase behavior

The order-parameter profile $\bar{Q}(\bar{r})$ that minimizes the free energy (1) is determined by $\delta F/\delta\bar{Q} = 0$, which yields the following Euler–Lagrange equation:

$$\frac{d\bar{f}}{d\bar{Q}} + \frac{6\bar{Q}}{\bar{r}^2} - \frac{2}{\bar{r}}\frac{d\bar{Q}}{d\bar{r}} - \frac{d^2\bar{Q}}{d\bar{r}^2} = 0, \tag{4}$$

together with boundary conditions

$$\left.\frac{d\bar{Q}}{d\bar{r}}\right|_{\bar{r}=\bar{R}_0} = -w, \tag{5}$$

$$\bar{Q}|_{\bar{r}=\infty} = 0. \tag{6}$$

Boundary condition (6) implies that the bulk is in the isotropic state. Note that in the nematic state, the spherical symmetry of our system with its radial order parameter profile is an artificial situation since it creates global splay deformation around the particle. We, therefore, restrict our discussion to the isotropic bulk state assuming $\tau > \tau_{\mathrm{IN}} = 1/8$.

The boundary-layer transition is monitored by a jump of the scalar order parameter at the surface, $\bar{Q}|_{\bar{r}=\bar{R}_0} = \bar{Q}_0$. In the planar case, which follows from our system for $\bar{R}_0 \to \infty$, the Euler–Lagrange equation, Eq. (4), with the vanishing second and third terms can be integrated at once and together with boundary condition (5), the surface order parameter follows from $[2\bar{f}(\bar{Q}_0)]^{1/2} = w$. When multiple solutions exist, the absolute minimum of the total free energy $\bar{F} = \int_0^{\bar{Q}_0}\{[2\bar{f}(\bar{Q})]^{1/2} - w\}d\bar{Q}$ has to be identified. Furthermore, a boundary-layer transition between different branches of minima is indicated in a Maxwell construction. This pathway, outlined by Sheng [15] and by Cahn [4], is no longer possible for curved surfaces. A first integral of Eq. (4) no longer exists. This is obvious from mechanical analogy with the replacement of $\bar{Q} \to x$ and $\bar{r} \to t$, where the second and third terms of Eq. (4) represent a time dependent potential and a friction term, respectively [7,9]. Instead, we follow a method outlined in Refs. [6] and [8] and use it in a version introduced in Ref. [9]. We solve Eq. (4) for fixed $\bar{Q}_0$ at the particle surface. We thus arrive at a family of orientational profiles for which we calculate the free energy $\bar{F}(\bar{Q}_0)$ which is now a function in the variable $\bar{Q}_0$. On the other hand, we consider the variation $\delta\bar{F}$ of our free energy within the family of profiles, just introduced. Since these profiles satisfy the bulk Euler–Lagrange equation, Eq. (4), the bulk term in the variation vanishes and the surface term gives

$$\frac{d\bar{F}(\bar{Q}_0)}{d\bar{Q}_0} = -\left.\frac{d\bar{Q}}{d\bar{r}}\right|_{\bar{r}=\bar{R}_0} - w, \tag{7}$$

where we replaced $\delta\bar{F}$ by $d\bar{F}(\bar{Q}_0)$. The condition $d\bar{F}/d\bar{Q}_0 = 0$ for a minimum of the total free energy $\bar{F}(\bar{Q}_0)$ then reproduces boundary condition (5). So if we plot $-(d\bar{Q}/d\bar{r})|_{\bar{r}=\bar{R}_0}$ as a function of $\bar{Q}_0$, the possible surface order parameters are the intersections with the constant w (see Fig. 2). Their free energies are calculated by integrating Eq. (7) and the absolute minimum of $\bar{F}(\bar{Q}_0)$ then gives the stable surface-order parameter $\bar{Q}_0$.

Suppose we find two solutions, $\bar{Q}_1$ and $\bar{Q}_2$, of Eq. (5), then a first-order phase transition between the branches of the two minima occurs if

$$\bar{F}(\bar{Q}_2) - \bar{F}(\bar{Q}_1) = \int_{\bar{Q}_1}^{\bar{Q}_2} d\bar{Q}_0 \left\{ -\left.\frac{d\bar{Q}}{d\bar{r}}\right|_{\bar{r}=\bar{R}_0} - w \right\} = 0. \tag{8}$$

This is a variant of Maxwell's construction illustrated in Fig. 2; since the two shaded regions possess equal areas, the boundary-layer transition takes place. Note that the third solution, $\bar{Q}_3$, corresponds to a maximum of the free energy and is therefore unstable. If surface constant w decreases relative

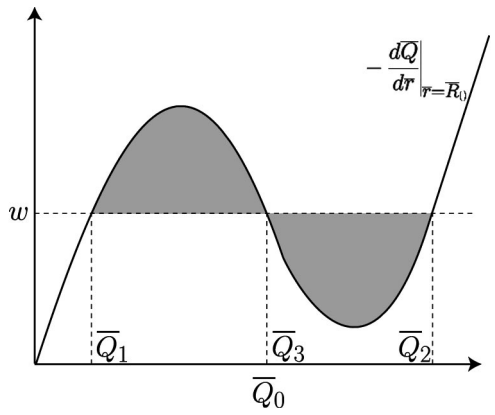

FIG. 2. Illustration of generalized Maxwell construction [see Eq. (8)]. The first-order surface-layer transition occurs between the small thin-layer ($\overline{Q}_1$) and the large thick-layer ($\overline{Q}_2$) order parameters when the areas of the two shaded regions are equal.

to the value in Fig. 2, thin-layer parameter $\overline{Q}_1$ is stable, whereas thick-layer parameter $\overline{Q}_2$ is realized for increasing w.

The critical points in the phase diagram of Fig. 1 occur when $(d\overline{Q}/d\overline{r})|_{\overline{r}=\overline{R}_0}$ as a function of $\overline{Q}_0$ possesses a saddle point [see Figs. 3(a)–3(c)],

$$\left.\frac{\partial}{\partial\overline{Q}_0}\frac{d\overline{Q}}{d\overline{r}}\right|_{\overline{r}=\overline{R}_0}=\left.\frac{\partial^2}{\partial\overline{Q}_0^2}\frac{d\overline{Q}}{d\overline{r}}\right|_{\overline{r}=\overline{R}_0}=0, \tag{9}$$

which determines the "critical temperature" τ^*. By varying surface coupling parameter w, the number of possible solutions of boundary equation (5) changes from three to one or vice versa, so the "critical anchoring strength" w^* for a given particle radius $\overline{R}_0$ is the solution of Eq. (5) at the saddle point.

III. RESULTS

In Fig. 3, we show plots of $-(d\overline{Q}/d\overline{r})|_{\overline{r}=\overline{R}_0}$ as a function of $\overline{Q}_0$ for various particle radii $\overline{R}_0$. The parameter of the curves in each plot is the temperature. In Fig. 3(a), we present, as a reference, the results for $\overline{R}_0=\infty$, i.e., a planar surface. Note that in this case the single curves can be determined completely analytically [15]. At the bulk transition temperature $\tau_{\mathrm{IN}}=0.125$, the derivative $-(d\overline{Q}/d\overline{r})|_{\overline{r}=\overline{R}_0}$ becomes zero for bulk order parameter $\overline{Q}_b$. The critical point in the phase diagram of Fig. 1 is given by the superheating temperature $\tau^*=9/64=0.140\,625$ and $w^*=9/128\simeq 0.0703$. For $\tau>\tau^*$, the curves are monotonic functions of $\overline{Q}_0$.

A large but finite radius of $\overline{R}_0=200$ is chosen in Fig. 3(b). Although it is similar to that in Fig. 3(a), the derivative $-(d\overline{Q}/d\overline{r})|_{\overline{r}=\overline{R}_0}$ never reaches zero for any finite $\overline{R}_0$. This is partly due to the effective shift in temperature, mentioned earlier in the discussion following Eq. (3).

Critical radius $\overline{R}_0^*$, where the length of the prewetting line shrinks to zero, is determined by the requirement that critical condition (9) is satisfied at $\tau=\tau_{\mathrm{IN}}$. We numerically obtain $\overline{R}_0^*\simeq 28.9$, and the appropriate plot is presented in Fig. 3(c). For any $\overline{R}_0<\overline{R}_0^*$ [see Fig. 3(d) for $\overline{R}_0=10$], the curves are monotonic functions for all $\tau>\tau_{\mathrm{IN}}$. Therefore, a boundary-layer transition can no longer occur. On the basis

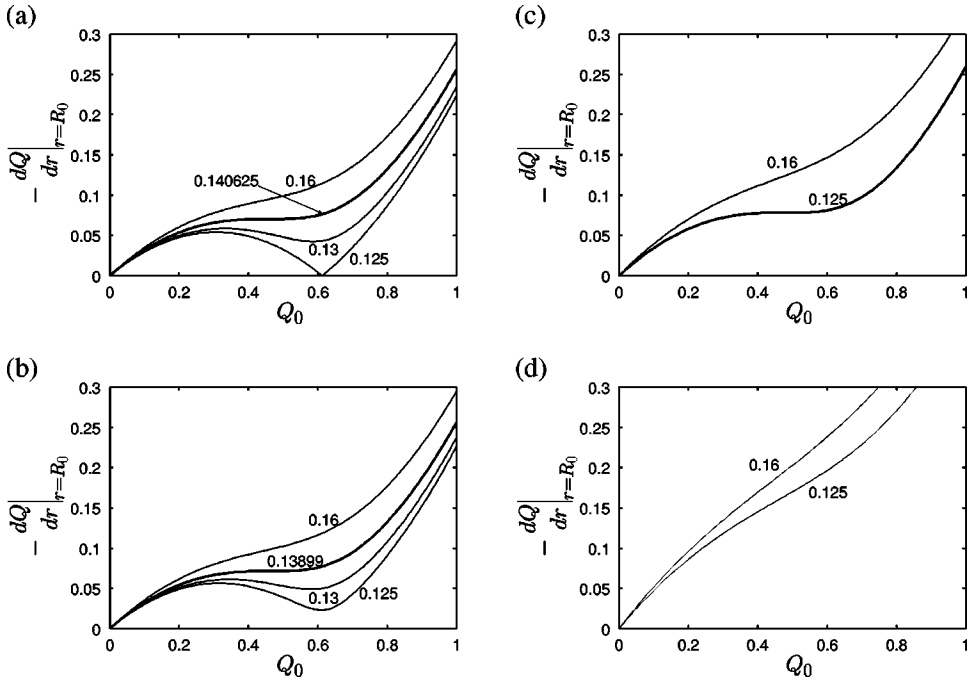

FIG. 3. Plots of $-(d\overline{Q}/d\overline{r})|_{\overline{r}=\overline{R}_0}$ vs $\overline{Q}_0$ for various particle radii: $\overline{R}_0=$ (a) ∞ (planar surface), (b) 200, (c) 28.9 (critical radius), and (d) 10. The numbers on the lines indicate τ. The curves at the critical temperature τ^* are plotted as thick lines.

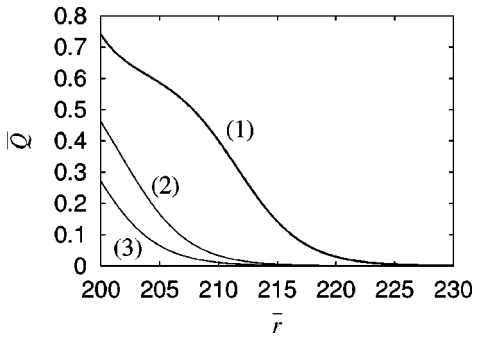

FIG. 4. Scalar order parameter $\bar{Q}$ as a function of radial distance $\bar{r}$ (measured from the center of the sphere) for $\bar{R}_0=200$ and $w=0.06$. Curve (1) is at τ_{IN}. Curves (2) and (3) are the respective thick-film and thin-film profiles right at the prewetting line for $\tau=0.132\,24$.

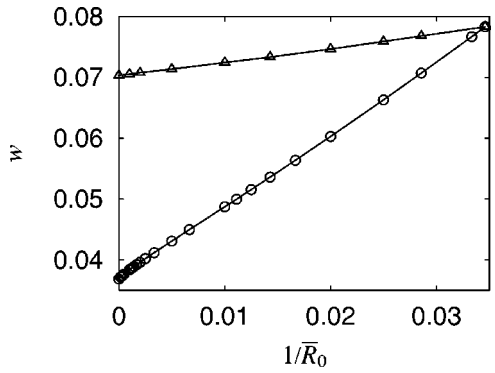

FIG. 5. Critical anchoring strength w^* (triangles) and anchoring strength w_t (circles), where the prewetting line intersects the coexistence line at τ_{IN}, plotted as a function of $1/\bar{R}_0$. As a guide to the eye, the lines connect the numerical data points.

of the plots in Fig. 3, we determined the phase diagram of Fig. 1, which shows the prewetting lines for different particle radii, as already discussed in Sec. I.

For typical nematic mesogens, the nematic coherence length $2\sqrt{2}\xi_n$ is of the order of 10 nm [26], so in real units the critical radius becomes $R_0^*\simeq 100$ nm. This means that in colloidal dispersions with particle radii larger than approximately 100 nm, the boundary-layer transition should be observable.

In Fig. 4 we illustrate the order-parameter profiles for the reduced particle radius $\bar{R}_0=200$ and surface-coupling parameter $w=0.06$ by plotting the scalar order parameter $\bar{Q}$ as a function of radial distance $\bar{r}$ (measured from the center of the sphere). At the bulk transition temperature $\tau_{\mathrm{IN}}=0.125$ [see curve (1)], the order parameter decays on a length scale of about four times the nematic coherence length $2\sqrt{2}\xi_n$, indicating that the particle is wetted by the nematic phase. However, due to the spherical geometry, complete wetting cannot occur since the surface tension at the interface between nematic and isotropic phases grows as $\bar{r}^2$. Curves (2) and (3) show the respective thick-film and thin-film solutions right at the prewetting line at reduced temperature of $\tau=0.132\,24$. The discontinuity in the surface order parameter is clearly visible.

In the following, we discuss further details of the prewetting line. From Fig. 1 we know that the possible anchoring strengths w where a boundary-layer transition occurs are bounded from above by the critical value w^* and from below by a value which we denote by w_t. At anchoring strength w_t, the prewetting line intersects the coexistence line at the bulk transition temperature, $\tau_{\mathrm{IN}}=0.125$. Or, mathematically speaking, for τ_{IN} condition (8) of Maxwell's construction is fulfilled at w_t. In Fig. 5 we plot both w^* and w_t as a function of the inverse particle radius, $1/\bar{R}_0$. We find that the dependence of w^* on the particle radius is rather weak and that the width of the region bounded by the two curves (where boundary-layer transitions occur) decreases almost linearly with $1/\bar{R}_0$. If we view the effect of curvature on this width as expansion in terms of $1/\bar{R}_0$, this means that the linear term is far more dominant than the higher-order contributions, which is reasonable for $\bar{R}_0>\bar{R}_0^*\simeq 28.9$.

Finally, in Fig. 6, we plot the critical temperature τ^* as a function of $1/\bar{R}_0$ (see the plus symbols). We notice again that, for the planar surface $(1/\bar{R}_0=0)$, the critical temperature $\tau^*_{\mathrm{planar}}=9/64=0.140\,625$ coincides with the superheating temperature of the nematic phase. Now, the decrease of τ^* with increasing curvature $(1/\bar{R}_0)$ reflects suppression of the boundary-layer transition due to elastic deformation in the order parameter induced by the curved surface of the particle. To show that distortion of the director field contributes significantly to this decrease, we present the following estimate. The linear part of the Euler–Lagrange equation, Eq. (4), reads $\bar{Q}\{\tau+6/\bar{r}^2-(2/\bar{r})(d\bar{Q}/d\bar{r})/\bar{Q}\}-(d^2\bar{Q}/d\bar{r}^2)=0$. The first and the fourth terms already appear in planar geometry. The second term results from distortion of the director field. It is, therefore, specific to the nematic problem. For thicknesses of the wetting layer much smaller than the particle radius, we can approximate it by $6/\bar{R}_0^2$. The third term also appears when critical wetting is studied in systems with a scalar order parameter. From the profiles in Fig. 3, we observe that, at the critical temperature, $d\bar{Q}/d\bar{r}|_{\bar{r}=\bar{R}_0}$ and $\bar{Q}_0$ only weakly depend on $1/\bar{R}_0$. With $d\bar{Q}/d\bar{r}|_{\bar{r}=\bar{R}_0}\simeq -0.07$,

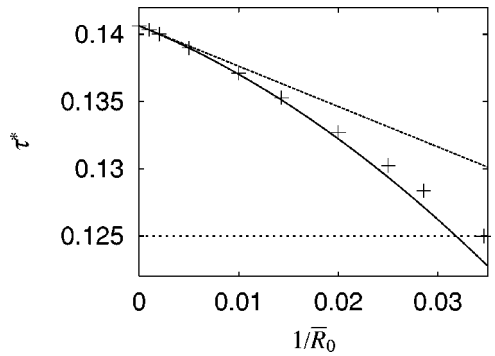

FIG. 6. Critical temperature τ^* (+) as a function of the inverse particle radius $1/\bar{R}_0$. The horizontal dotted line indicates the bulk transition temperature $\tau_{\mathrm{IN}}=0.125$. The solid and dashed lines are estimates for τ^* (see the text for details).

$\bar{Q}_0^* \simeq 0.46$, and $1/\bar{r} \to 1/\bar{R}_0$, we write the third term as $0.3/\bar{R}_0$. The second and third terms can now be viewed as an effective shift in temperature due to curvature which approximately reads $\delta\tau \simeq 6/\bar{R}_0^2 + 0.3/\bar{R}_0$. We use it to estimate the critical temperature as $\tau^* = \tau^*_{\text{planar}} - \delta\tau = 9/64 - 6/\bar{R}_0^2 - 0.3/\bar{R}_0$ which corresponds to the solid line in Fig. 6. It represents a good estimate of the numerical data. Deviations grow with an increase of $1/\bar{R}_0$, as expected. If we just retain the linear term in $1/\bar{R}_0$, which appears in scalar-order-parameter theory, the dashed line results. In comparing both lines, it is obvious that distortion of the director field, specific to nematic liquid crystals, has a non-negligible effect on the wetting of curved surfaces.

IV. CONCLUSION

Using generalized Maxwell construction, we discussed the boundary-layer transition in a nematic liquid crystal surrounding a spherical particle above the bulk isotropic–nematic transition temperature. For varying particle radii, we determined the prewetting line to be a function of the temperature and the surface-coupling parameter. The prewetting line ends at a critical point. Furthermore, it shrinks with a decrease in particle radius and vanishes completely below a critical radius of the order of 100 nm. In contrast to conventional systems studied so far, with their scalar order parameter (e.g., binary fluids), the nematic tensor order parameter allows elastic distortion in the preferred orientational axis (director field). Splay deformation in the nematic wetting layer around spherical particles gives rise to an effective shift in temperature. Based on this interpretation, we introduced a good estimate for the critical temperature as a function of the inverse particle radius. It demonstrates that director distortions significantly alter the prewetting transition compared to standard scalar-order-parameter theory [9].

Several extensions of this work are possible. The first is to take the Nobili–Durand surface free energy $[W(Q_{\alpha\beta} - Q^{(0)}_{\alpha\beta})^2/2]$ which is quadratic in the tensor order parameter [28]. As we already pointed out, the main goal of this article was to introduce a method by which to study boundary-layer transitions in the presence of curvature and to clarify the main consequences of curvature. We do not expect dramatic changes when using Nobili–Durand surface free energy. For uniaxial homeotropic anchoring it becomes $W(Q - Q_s)^2/2$ that contains two parameters, the anchoring strength W and the preferred scalar surface order parameter Q_s. We already know the boundary-layer phase diagram in this case for a planar surface [16,29]: for Q_s smaller than the bulk value Q_b of the nematic phase, complete wetting cannot occur. Above Q_b the prewetting line becomes a surface in the temperature-Q_s-W phase diagram which ends in a critical line. We expect this surface to vanish gradually with an increase in inverse particle radius.

A second extension concerns temperatures below τ_{IN}. We already pointed out that splay distortions close to a spherical particle introduce a shift in temperature which also lowers the isotropic–nematic transition temperature. It would be interesting to study the consequences for orientational order around the particle. However, our assumption of radial symmetry no longer makes sense since far from the particle, where the liquid crystal has already condensed into nematic phase, a radial director field is unrealistic. On the other hand, with the more realistic uniform director field at infinity, we no longer have an effective one-dimensional problem, so the complexity of the problem increases. Nevertheless, some insight into this modified system could also add to understanding of the properties of recently observed soft solids [30], i.e., cellular structures whose walls are made up of particle agglomerates and whose cells are filled by nematic phase. Of course, deep in the nematic phase typical configurations around a spherical particle will occur [31].

As a third extension, one can also study planar anchoring of liquid crystal molecules. In the case of a planar substrate this was done by Sluckin and Poniewierski [17] who discussed a wealth of new phenomena, including the occurrence of a biaxial surface state and the possibility of a Kosterlitz–Thouless–Halperin–Nelson–Young transition. It would be interesting to extend the study to curved surfaces, especially spheres and for a uniaxial order parameter, where the topology requires the existence of surface defects with total charge of $+2$ [32]. In a purely two-dimensional (2D) nematic, the total charge is realized by four $+1/2$ disclinations sitting on the vertices of a tetrahedron [33]. In the case of wetting layers, we can show that for appropriate surface coupling parameters the four $+1/2$ disclinations still exist but are realized by a biaxial order parameter field [34].

Before concluding this article we want to comment on experimental observation of nematic wetting layers of isolated spheres and the effect of curvature on the prewetting line. Clearly, the wetting layer affects the Stokes drag of a particle and hence its Brownian motion since they are observable with dynamic light scattering in conventional colloidal dispersions [35]. Early experiments on liquid crystal colloids using dynamic light scattering detected an increase in Stokes drag close to the isotropic–nematic transition [36]. We suggest the use of more refined experiments with varying particle radii to examine the details reported in this article. Quantitative predictions for Stokes drag have to be based on dynamic equations that involve the tensorial order parameter [37] so, therefore, they present a more complicated problem. Based on our knowledge of Stokes drag deep in the nematic phase [38], we are currently thinking along this line.

Considering the recent growing interest in liquid crystal colloidal dispersions, we hope that this article stimulates further experimental as well as theoretical studies on wetting phenomena in these systems.

ACKNOWLEDGMENTS

The authors thank R. Evans and especially W. Poon. Discussions with the latter initiated this work. One of the authors (H.S.) thanks the Yokoyama Nano-structured Liquid Crystal Project for generous financial support during his stay in Tsukuba. He also acknowledges financial support by the Deutsche Forschungsgemeinschaft under Grant No. Sta 352/5-1.

[1] See the webpage: http://www.botanik.uni-bonn.de/system/bionik.htm.
[2] S. Dietrich, in *Phase Transitions and Critical Phenomena*, edited by C. Domb and J. Lebowitz (Academic, London, 1988), Vol. 12.
[3] M. Schick, in *Liquids at Interfaces, Les Houches, Session XLVIII, 1988*, edited by J. Charvolin, J. F. Joanny, and J. Zinn-Justin (Elsevier Science, Amsterdam, 1990).
[4] J.W. Cahn, J. Chem. Phys. **66**, 3667 (1977).
[5] H. Nakanishi and M.E. Fisher, Phys. Rev. Lett. **49**, 1565 (1982); R. Lipowsky, *ibid.* **49**, 1575 (1982); R. Lipowsky and W. Speth, Phys. Rev. B **28**, 3983 (1983).
[6] P. Levinson, J. Jouffroy, and F. Brochard, J. Phys. (France) Lett. **46**, L-21 (1985).
[7] R. Holyst and A. Poniewierski, Phys. Rev. B **36**, 5628 (1987).
[8] M.P. Gelfand and R. Lipowsky, Phys. Rev. B **36**, 8725 (1987).
[9] J.O. Indekeu, P.J. Upton, and J.M. Yeomans, Phys. Rev. Lett. **61**, 2221 (1988); P.J. Upton, J.O. Indekeu, and J.M. Yeomans, Phys. Rev. B **40**, 666 (1989).
[10] T. Bieker and S. Dietrich, Physica A **252**, 85 (1998); R. Evans, R. Roth, and P. Bryk, Europhys. Lett. **62**, 815 (2003).
[11] D. Beysens and D. Estève, Phys. Rev. Lett. **54**, 2123 (1985).
[12] P. Taborek and L. Senator, Phys. Rev. Lett. **57**, 218 (1986).
[13] B. Jérôme, Rep. Prog. Phys. **54**, 391 (1991).
[14] For a collection of references, see, for example, I. Lelidis and P. Galatola, Phys. Rev. E **66**, 010701(R) (2002).
[15] P. Sheng, Phys. Rev. A **26**, 1610 (1982).
[16] A. Poniewierski and T.J. Sluckin, Mol. Cryst. Liq. Cryst. **111**, 373 (1984); **126**, 143 (1984); Liq. Cryst. **2**, 281 (1987).
[17] T.J. Sluckin and A. Poniewierski, Phys. Rev. Lett. **55**, 2907 (1985); in *Fluid Interfacial Phenomena*, edited by C. A. Croxton (Wiley, New York, 1986).
[18] K. Miyano, Phys. Rev. Lett. **43**, 51 (1979).
[19] H. Yokoyama, S. Kobayashi, and H. Kamei, Mol. Cryst. Liq. Cryst. **99**, 39 (1983).
[20] M.I. Boamfa, M.W. Kim, J.C. Maan, and Th. Rasing, Nature (London) **421**, 149 (2003).
[21] R. van Roij, M. Dijkstra, and R. Evans, Europhys. Lett. **49**, 350 (2000); M. Dijkstra, R. van Roij, and R. Evans, Phys. Rev. E **63**, 051703 (2001).
[22] A. Borštnik, H. Stark, and S. Žumer, Phys. Rev. E **60**, 4210 (1999); **61**, 2831 (2000).
[23] K. Kočevar and I. Muševič, Phys. Rev. E **64**, 051711 (2001); K. Kočevar, A. Borštnik, I. Muševič, and S. Žumer, Phys. Rev. Lett. **86**, 5914 (2001).
[24] P. Galatola and J.-B. Fournier, Phys. Rev. Lett. **86**, 3915 (2001); H. Stark, Phys. Rev. E **66**, 041705 (2002); P. Galatola, J.-B. Fournier, and H. Stark, *ibid.* **67**, 031404 (2003).
[25] The wetting surface-coupling parameter w_m can be calculated analytically for planar geometry. The result is $w_m = 1/32\sqrt{-9+6\sqrt{3}} \simeq 0.036\,87$.
[26] P.G. de Gennes and J. Prost, *The Physics of Liquid Crystals*, 2nd ed. (Oxford University Press, Oxford, 1993).
[27] S. Hess, Z. Naturforsch. A **30A**, 728 (1975).
[28] M. Nobili and G. Durand, Phys. Rev. A **46**, R6174 (1992).
[29] J. Fukuda, H. Stark, and H. Yokoyama (unpublished results).
[30] S.P. Meeker, W.C.K. Poon, J. Crain, and E.M. Terentjev, Phys. Rev. E **61**, R6083 (2000); V.J. Anderson, E.M. Terentjev, S.P. Meeker, J. Crain, and W.C.K. Poon, Eur. Phys. J. E **4**, 11 (2001); V.J. Anderson and E.M. Terentjev, *ibid.* **4**, 21 (2001).
[31] H. Stark, Phys. Rep. **351**, 387 (2001).
[32] M.V. Kurik and O.D. Lavrentovich, Sov. Phys. Usp. **31**, 196 (1988) [Usp. Fiz. Nauk **154**, 381 (1988)].
[33] T.C. Lubensky and J. Prost, J. Phys. II **2**, 371 (1992); D.R. Nelson, Nano Lett. **2**, 1125 (2002).
[34] M. Huber and H. Stark (unpublished results).
[35] B.J. Berne and R. Pecora, *Dynamic Light Scattering—With Applications to Chemistry, Biology, and Physics* (Wiley, New York, 1976).
[36] A. Böttger, D. Frenkel, E. van de Riet, and R. Zijlstra, Liq. Cryst. **2**, 539 (1987).
[37] S. Hess, Z. Naturforsch. A **30A**, 728 (1975); N. Kuzuu and M. Doi, J. Phys. Soc. Jpn. **52**, 3486 (1983); P.D. Olmsted and P.M. Goldbart, Phys. Rev. A **41**, 4578 (1990); B.J. Edwards, A.N. Beris, and M. Grmela, Mol. Cryst. Liq. Cryst. **201**, 51 (1991); T. Qian and P. Sheng, Phys. Rev. E **58**, 7475 (1998); H. Pleiner, M. Liu, and H.R. Brand, Rheol. Acta **41**, 375 (2002); H. Stark and T.C. Lubensky, Phys. Rev. E **67**, 061709 (2003).
[38] H. Stark and D. Ventzki, Phys. Rev. E **64**, 031711 (2001); Europhys. Lett. **57**, 60 (2002); H. Stark, D. Ventzki, and M. Reichert, J. Phys.: Condens. Matter **15**, S191 (2003).